

Distinctive electron localization on the surface of two-dimensional antiferromagnetic metal $PdCrO_2$

Jing-Zhi Chen(陈景芝), Yu-Jing Ren(任宇靖), Peng-Hao Yuan(袁鹏浩), Li-Li Meng(孟丽丽), Yu Zhu(朱玉), Yi Ou(欧仪), and Yan Zhang(张焱)

Citation: Chin. Phys. B, 2026, 35 (**6**): 067302. DOI: 10.1088/1674-1056/ae4c65
http://cpb.iphy.ac.cn; http://iopscience.iop.org/cpb

What follows is a list of articles you may be interested in

Type-II Dirac nodal chain semimetal CrB_4

Xiao-Yao Hou(侯逍遥), Ze-Feng Gao(高泽峰), Peng-Jie Guo(郭朋杰), Jian-Feng Zhang(张建丰), and Zhong-Yi Lu(卢仲毅)
Chin. Phys. B, 2026, 35 (**1**): 017301. DOI: 10.1088/1674-1056/ae172b

Doping-induced magnetic and topological transitions in $Mn_2X_2Te_5$ (X = Bi, Sb) bilayers

Wei Chen(陈威), Chuhan Tang(唐楚涵), Chao-Fei Liu(刘超飞), and Mingxing Chen(陈明星)
Chin. Phys. B, 2025, 34 (**9**): 097304. DOI: 10.1088/1674-1056/ade4af

Phase changings in the surface layers of T_d-WTe_2 driven by alkali-metal deposition

Yu Zhu(朱玉), Zheng-Guo Wang(王政国), Yu-Jing Ren(任宇靖), Peng-Hao Yuan(袁鹏浩), Jing-Zhi Chen(陈景芝), Yi Ou(欧仪), Li-Li Meng(孟丽丽), and Yan Zhang(张焱)
Chin. Phys. B, 2025, 34 (**1**): 017302. DOI: 10.1088/1674-1056/ad9e9e

Dynamic localization of two electrons in AC-driven triple quantum dots and quantum dot shuttles

Jin-Xian Qu(屈晋先), Su-Qing Duan(段素青), Ning Yang(杨宁)
Chin. Phys. B, 2017, 26 (**12**): 127308. DOI: 10.1088/1674-1056/26/12/127308

Quantum transport through a Z-shaped silicene nanoribbon

A Ahmadi Fouladi
Chin. Phys. B, 2017, 26 (**4**): 047304. DOI: 10.1088/1674-1056/26/4/047304

RAPID COMMUNICATION

Distinctive electron localization on the surface of two-dimensional antiferromagnetic metal $PdCrO_2$

Jing-Zhi Chen(陈景芝)[1], Yu-Jing Ren(任宇靖)[1], Peng-Hao Yuan(袁鹏浩)[1], Li-Li Meng(孟丽丽)[1], Yu Zhu(朱玉)[1], Yi Ou(欧仪)[1], and Yan Zhang(张焱)[1,2,†]

[1] *International Center for Quantum Materials, School of Physics, Peking University, Beijing* 100871, *China*
[2] *Collaborative Innovation Center of Quantum Matter, Beijing* 100871, *China*

(Received 24 November 2025; revised manuscript received 1 February 2026; accepted manuscript online 3 March 2026)

Electron localization is a focal topic in condensed matter physics. In materials where electrons couple with lattice/spin degrees of freedom, an accurate characterization of electron localization would not only advance our understanding of correlated electron systems but also hold potential as a key to unraveling the long-standing puzzle of high-temperature superconductivity. Here, utilizing angle-resolved photoemission spectroscopy (ARPES), we reveal an electron localization that occurs on the surface of a two-dimensional antiferromagnetic metal $PdCrO_2$. Various characteristics of electron localization were observed, including quasiparticle mass renormalization, the "waterfall" feature, high-energy incoherent states, and a pseudogap. We find that the energy scale of band renormalization is highly correlated with the mode coupling energy observed in the metallic state, suggesting that the localization behavior can be explained by polaron localization driven by an enhancement of the coupling between electrons and lattice/spin excitations. Our data highlight phenomena that emerge universally in complex correlated systems where electrons couple with lattice/spin excitations. This provides experimental validation for various theoretical models of delocalized correlated systems. Our results also demonstrate that the coupling strength can be tuned continuously on the surface of $PdCrO_2$, making it a model system for investigating exotic phenomena in complex correlated materials.

Keywords: angle-resolved photoemission spectroscopy, delafossite oxides, electron localization

PACS: 73.20.At, 71.30.+h, 79.60.–i

DOI: 10.1088/1674-1056/ae4c65 **CSTR:** 32038.14.CPB.ae4c65

In the research of condensed matter physics, it has been found that the insulating properties of certain materials cannot be explained by the band theory. These findings have stimulated research into the underlying mechanisms of electron localization.[1] Localization mechanisms, such as Anderson localization driven by disorder scatterings,[1,2] and Mott localization driven by Coulomb repulsive interactions,[1,3] have built the foundation for our understanding of correlated electron systems. Later, the discovery of high-temperature superconductivity in cuprates shifted the focus of research from localization itself to the entire transition process from a localized insulating state to a delocalized metallic state.[4] It has been widely accepted that a comprehensive understanding of the behaviors of holes or electrons in doped Mott insulators may hold the key to unraveling the mechanism of high-temperature superconductivity. However, while fully localized states are reasonably well described by theories, there remains controversies regarding the theoretical descriptions of delocalized correlated states, or simply put, the electrons or holes moving in a correlated insulating background. Several theoretical models with different emphases have been proposed, such as resonating valence bond (RVB) theory,[5] stripe theory,[6] spin polaron theory,[7,8] etc. The challenges in resolving the theoretical controversies lie in, on one hand, the calculational difficulties inherent in simultaneously accounting for multiple degrees of freedom. On the other hand, the detailed experimental characterization of low-energy excitations that cover the entire transition process from localized to delocalized states is lacking. Angle-resolved photoemission spectroscopy (ARPES) is a powerful tool for probing the single-particle excitation spectral function of materials. However, limited by the difficulties in synthesizing high-quality samples with specific doping levels, there are very few systems in which ARPES measurements could be conducted in the entire doping range that covers the localized-to-delocalized transition.[9–11]

$PdCrO_2$, together with its sister compound $PdCoO_2$, is a quasi-two-dimensional layered material that attracts great attention for its low electric resistivity at room temperature.[12,13] Studies on Pd(Cr, Co)O_2 have found that Pd exhibits a rare +1 oxidation state with a $4d^9$ electron configuration. Meanwhile, due to the dumbbell O–Pd–O bond configuration, the Pd d-electrons form a two-dimensional conductive layer in Pd(Cr, Co)O_2 with excellent metallic properties.[12,14] In contrast to the metallic nature of the Pd

†Corresponding author. E-mail: yzhang85@pku.edu.cn

© 2026 Chinese Physical Society and IOP Publishing Ltd. All rights, including for text and data mining, AI training, and similar technologies, are reserved.

layer, the CoO_2 and CrO_2 layers exhibit insulating properties. The difference lies in that the electron configuration of Co^{3+} in the CoO_2 layer is $3d^6$, which belongs to a band insulator with an even number of valence electrons; whereas the electron configuration of Cr^{3+} in the CrO_2 layer is $3d^3$, which belongs to a Mott insulator.[12,15,16] Experiments have shown that the CrO_2 layer in $PdCrO_2$ exhibits large magnetic moments and strong magnetic fluctuations.[17–19] A complex 120° antiferromagnetic order with a Néel temperature of ~ 37.5 K was found in the CrO_2 layer of $PdCrO_2$.[17–19]

Compared with the complex octahedral distortion commonly existing in perovskite-structured oxides, $PdCrO_2$ has a relatively simple and regular lattice structure.[13] Meanwhile, its antiferromagnetic insulating CrO_2 layers and metallic Pd layers are spatially separated. This makes $PdCrO_2$ an ideal system for studying the interactions between itinerant electrons and the correlated insulating background. However, transport and ARPES studies show that the coupling between the itinerant electrons in the Pd layers and the correlated electrons in the CrO_2 layers is relatively weak in bulk samples.[20–22] On one hand, the two-dimensionality of Pd d-electrons limits their coupling with the adjacent CrO_2 layers. On the other hand, due to the opening of a Mott gap, the low-energy excitations of the CrO_2 layers are distributed far away from the Fermi energy (E_F) and do not overlap with the itinerant Pd d-electrons.[15,16,23]

While the coupling between itinerant and localized electrons is weak in bulk $PdCrO_2$, distinctive surface electronic states have been found in Pd(Cr, Co)O_2.[21,24–26] The cleavage surface of Pd(Cr, Co)O_2 consists of two different surface terminations. Due to the surface polarization effect, the Pd-terminated surface has 0.5 more electrons than the bulk Pd layers, whereas the (Cr, Co)O_2-terminated surface has 0.5 more holes. This results in the formation of surface electronic states in Pd(Cr, Co)O_2 that are distinct from the bulk. ARPES studies on $PdCoO_2$ have observed electron-type and hole-type surface states on the Pd- and CoO_2-terminated surfaces, respectively, confirming the existence of surface electronic states due to surface polarization.[24,25] Moreover, researchers have found that the surface electronic states may be spin polarized due to the formation of surface ferromagnetism.[25] Self-energy analysis has found evidence for the existence of electron–magnon coupling in the surface electronic states of $PdCoO_2$.[26]

Here, we study the Pd-terminated surface of $PdCrO_2$ using small-spot ARPES. A circular electron-like pocket was resolved at the Brillouin zone center with a parabolic band dispersion. A kink feature was resolved at ~ -200 meV, which manifests the existence of electron-boson coupling at this specific energy. As the sample temperature increases, we find that the surface electronic state undergoes a transition from an itinerant metallic state to a localized insulating state. Various characteristics of electron localization were observed including mass renormalization, the "waterfall" feature, high-energy incoherent states, and a pseudogap. The energy scale of band renormalization was found to be highly correlated with the ~ 200 meV mode-coupling energy. This suggests that the electron localization we observed cannot be explained by simple Anderson localization or the suppression of photoemission intensity caused by disorder or surface degradation, but rather by the localization of lattice-/spin-polarons. Our data highlight the universal phenomena that emerge in the electron localization process of a complex correlated system. The quantitative characterization of these phenomena provides experimental evidence for validating theoretical models of delocalized correlated systems. Meanwhile, our results indicate that the coupling strength between electrons and lattice/spin excitations can be tuned continuously from weak to strong on the surface of $PdCrO_2$, making it an ideal system for studying the coupling between delocalized electrons and lattice/spin excitations in complex correlated systems.

Single crystals of $PdCrO_2$ were synthesized using the flux method.[13] ARPES measurements were performed at the BL03U beamline of the Shanghai Synchrotron Radiation Facility (SSRF) using a photon energy of 55 eV. A Scienta DA30L analyzer was used, with an overall energy resolution of ~ 12 meV and an angular resolution of $\sim 0.3°$. The crystals were cleaved *in situ* at a temperature of 10 K with a chamber pressure lower than 6×10^{-11} mbar. A momentum-independent background was subtracted from the photoemission data to remove the background signal originating from secondary scatterings of photoelectrons.

Previous ARPES studies on $PdCoO_2$ have shown that the Pd surface states contribute to two Fermi pockets at the Brillouin zone center.[25] Using small-spot ARPES, we optimized the beam spot position to target the Pd-terminated surface as much as possible based on the photoemission intensity collected at the Brillouin zone center. It should be noted that the spot size we used is around 100 μm,[27] which is not necessarily smaller than the domain size of the Pd-terminated surface; thereby part of our photoemission signal may be contributed by the CrO_2-terminated surface. However, according to previous studies, the CrO_2 surface state is insulating with a large energy gap.[28,29] Therefore, the photoemission signal from the CrO_2-terminated surface would not complicate our characterization of the Pd surface electron states near E_F. Figure 1(a) presents the Fermi surface mapping measured at the optimized position for the Pd-terminated surface. The data are consistent with a previous ARPES study.[21] The outermost hexagonal Fermi pocket originates from the bulk electronic states (H-bulk), while the other two Fermi pockets — an inner hexagonal surface state (H-PSS) and a circular surface state (C-PSS) — derive from the Pd-terminated surface. Different

shapes of Fermi pockets indicate that the two surface states (H-PSS and C-PSS) may have different orbital compositions. The orbital composition of H-PSS is the Pd-e_g' orbital, which is the same as the H-bulk state.[15,30] For C-PSS, according to the theoretical calculation in $PdCoO_2$, its orbital composition is mainly composed of Pd–Co–O orbitals.[29] The focus of our subsequent work will be on C-PSS, which exhibits properties distinct from those of the H-PSS and H-bulk states.

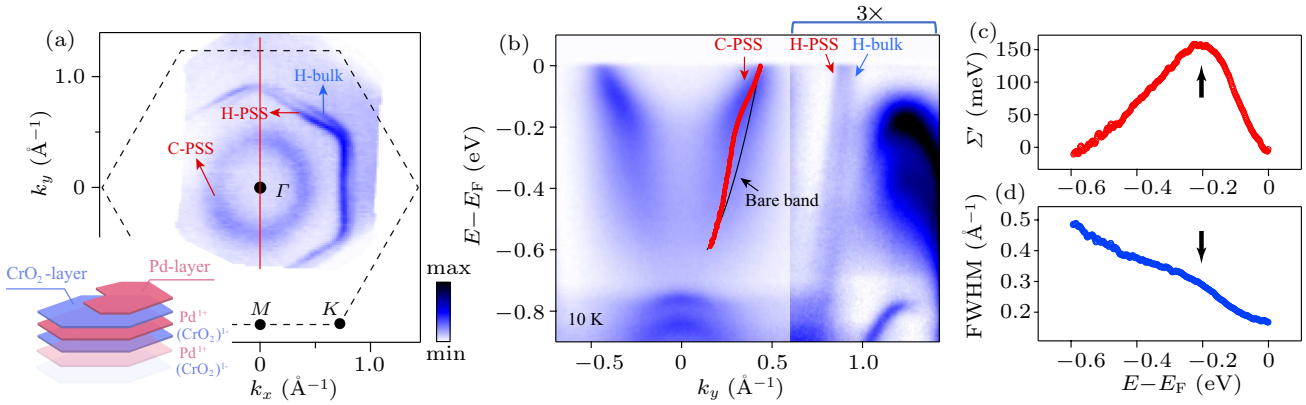


Fig. 1. Fermi surface mapping and band dispersion of the Pd surface state in $PdCrO_2$. (a) Fermi surface mapping of $PdCrO_2$. Red solid line shows the momentum position of the energy–momentum cut. Inset panel illustrates the polar surface of $PdCrO_2$ with two different terminations. (b) Energy–momentum cut taken along the Γ–M direction. Hexagonal bulk (H-bulk) state, hexagonal surface state (H-PSS), and circular surface state (C-PSS) are highlighted by the arrows in panels (a) and (b). The photoemission intensity of the right part of the image is enhanced by three times to better show the H-PSS and H-bulk states. Fitted and bare band dispersions are illustrated using red markers and black solid line, respectively. (c) Energy dependence of the real-part of self-energy (Σ'). (d) Energy dependence of the fitted full width at half maximum (FWHM) of momentum distribution curve (MDC) peaks. Black arrows in panels (c) and (d) highlight the mode coupling energy at ~ -0.2 eV. All data were taken using 55 eV photon energy at 10 K.

Figure 1(b) presents the measured band dispersion along the Γ–M direction. The band dispersion of C-PSS is parabolic and electron-like, with a distinct kink structure observed at ~ -0.2 eV. We obtained the C-PSS band dispersion by fitting the peak positions of the momentum distribution curves (MDCs) using a Lorentzian function. We calculated the real part of the self-energy (Σ') based on the fitted band dispersion (red markers) and a parabolic bare-band dispersion (black solid line). As shown in Fig. 1(c), the real part of the self-energy exhibits a broad peak at ~ -0.2 eV. For the imaginary part of the self-energy, due to possible extrinsic broadening of our spectra, we did not use the strict Kramers–Kronig relations to calculate it. Instead, we show the fitted full width at half maximum (FWHM) of the MDC peaks in Fig. 1(d), which reflects the energy dependence of the imaginary part of the self-energy to a certain extent. A significant increase in FWHM is observed at ~ -0.2 eV in Fig. 1(d). The above behaviors all indicate that the electrons of C-PSS couple with bosonic modes at an energy scale of approximately 200 meV. Such coupling is absent in the H-PSS and H-bulk states.

Figure 2 presents the temperature-dependent evolution of the band dispersion of the Pd surface state. To better identify the band dispersion, we performed a minimum gradient calculation,[31] and the results are shown in Fig. 2(b). Unlike the second derivative calculation, which normally highlights the band dispersion along either the energy or momentum direction, for our data that consist of both rapid and slow band dispersions, the minimum gradient calculation that highlights the local peak positions is more applicable. Both the raw data and the minimum gradient images clearly show that the C-PSS undergoes a metal-to-insulator transition, as manifested by various electron localization behaviors including the reduction of band width, the suppression of spectral weight at E_F, and the spectral weight transfer from low to high binding energy. It should be noted that previous ARPES studies on $PdCrO_2$ and $PdCoO_2$ have found that the surface states could be removed by performing thermal cycling treatment.[21,24] Here, we verified that the surface states did not recover to the metallic state after our temperature cycle (see Fig. S1 in the supplementary materials for details). This suggests that the role of the temperature increase in our experiment is not inducing thermal fluctuation, but rather is similar to that of increased cleavage time, which jointly drives an irreversible transition of electronic states from itinerant to localized on the Pd-terminated surface. To facilitate discussion, we still use temperature to denote the degree of progression of the electron localization in the following parts of this paper.

We now discuss different characteristics of the electronic structure in different energy ranges. First, in the low-energy range from the mode coupling energy (~ -0.2 eV) to E_F, a quasiparticle band (QPB) is observed. Its bandwidth decreases rapidly with the occurrence of electron localization, indicating a significant increase in the quasiparticle effective mass. At 100 K, the QPB is renormalized into a flat band with a bandwidth of ~ 100 meV. Second, in the high-energy range from -0.6 eV to -0.4 eV, the spectra exhibit a nearly single-electron excitation behavior in the metallic state at 10 K, following a parabolic band dispersion. However, in the insulating state at 100 K, the spectral weight is distributed over an extremely broad energy range, exhibiting an incoherent exci-

tation behavior. Such incoherent spectral weight forms a high-energy band (HEB) in the insulating state. Finally, in the intermediate energy region between the QPB and HEB, a "waterfall" feature that has been widely observed in cuprates[32,33] is observed at 70 K. In the metallic state, the entire band disperses continuously from −0.6 eV to E_F, while in the localized insulating state, the two bands, QPB and HEB, are well separated. In the intermediate stage of localization (70 K), the spectral weight is more concentrated in the QPB at large momenta near the Fermi crossings, while it is more concentrated in the incoherent HEB at small momenta near the Brillouin zone center. A "waterfall" distribution of spectral weight is thereby established in the momentum region where the QPB and HEB connect.

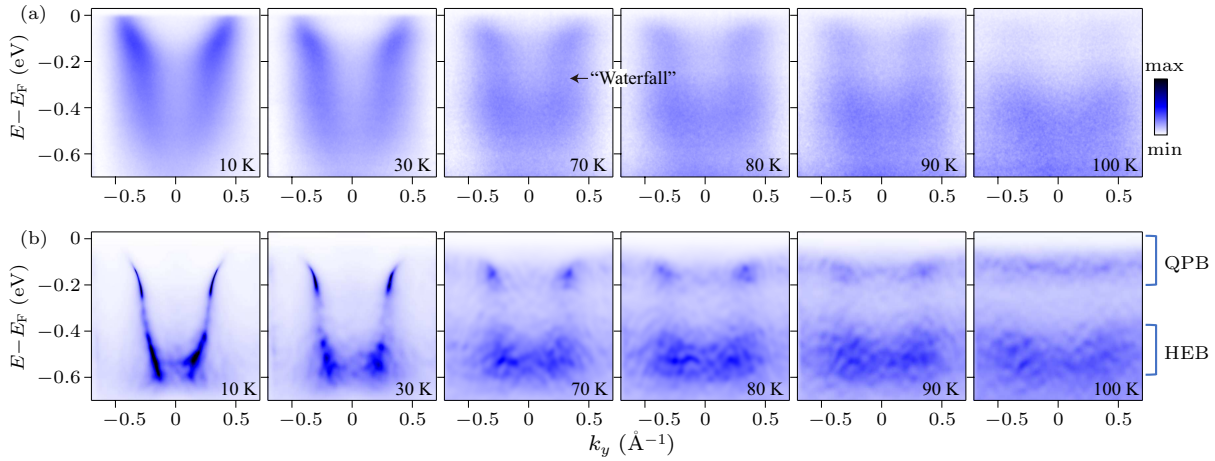


Fig. 2. Electron localization behaviors observed on the Pd surface state in $PdCrO_2$. (a) Temperature dependence of the energy–momentum cuts taken along the Γ–M direction. The formation of "waterfall" feature is highlighted in 70 K data. (b) Corresponding minimum gradient calculations[31] of the data in panel (a). The energy ranges of the quasi-particle band (QPB) and the high-energy band (HEB) are highlighted. The minimum gradient images of all measured temperature points are shown in Fig. S2 in the supplementary materials.

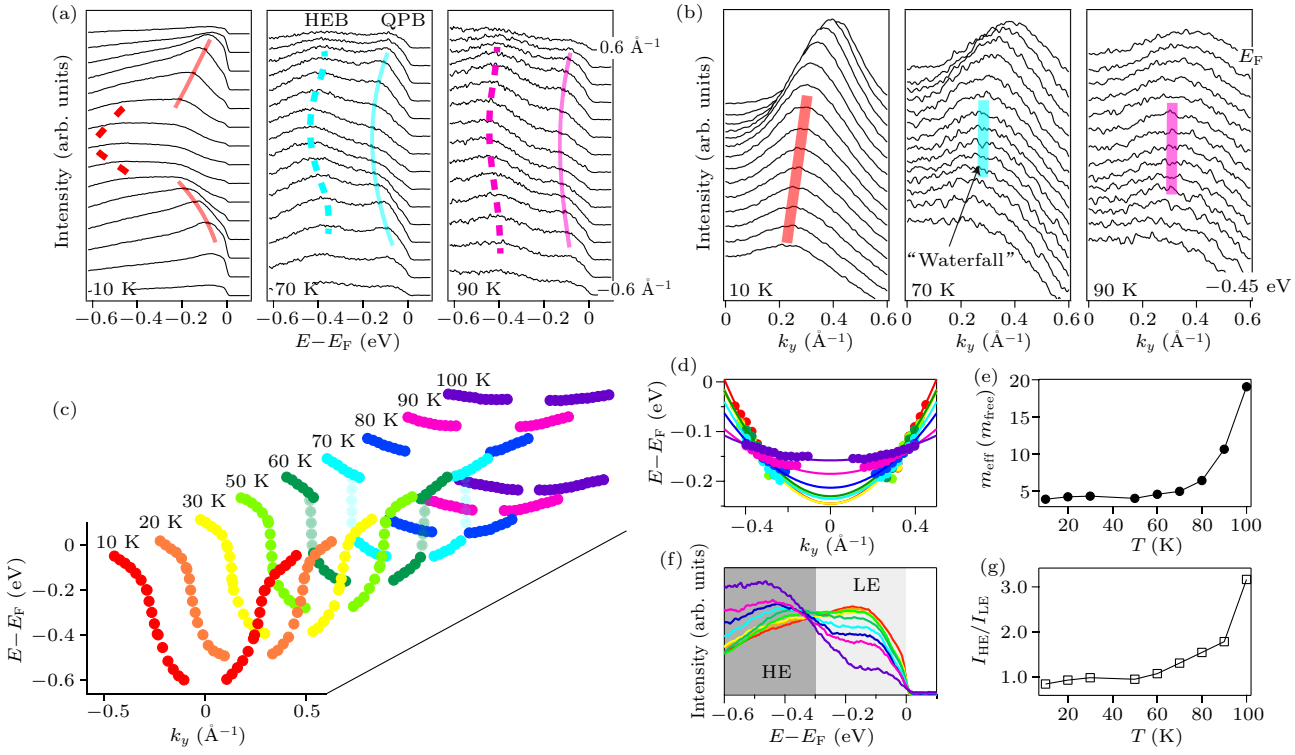


Fig. 3. Characterization of the band dispersion, effective mass, and spectral weight transfer. (a) Energy distribution curves (EDCs) extracted from the 10 K, 70 K, and 90 K data in the momentum region from −0.6 Å^{-1} to 0.6 Å^{-1}. Dashed and solid lines are intended to guide the eyes to the band dispersions of HEB and QPB, respectively. (b) MDCs extracted from the 10 K, 70 K, and 90 K data in the energy region from −0.45 eV to E_F. Shaded lines are intended to guide the eyes to the energy dependence of the MDC peak positions. (c) Band dispersions extracted based on the minimum gradient images (see Fig. S2 in thesupplementary materials for details). (d) Fitting of the QPB dispersions at different temperatures using a parabolic band dispersion. The fitting results are shown using solid lines. (e) Temperature dependence of the effective mass calculated using the data in panel (d). (f) Temperature dependence of the EDCs integrated in [0, 0.55] Å^{-1}. The high energy (HE) and low energy (LE) regions are illustrated using shaded areas. (g) Temperature dependence of the intensity ratio (I_{HE}/I_{LE}) calculated using the data in panel (f). The color coding of temperature is the same in panels (c), (d), and (f).

To better visualize the evolution of the electronic structure, we compared the energy distribution curves (EDCs) and MDCs at three representative temperatures of 10 K, 70 K, and 90 K in Figs. 3(a) and 3(b). We could directly observe the renormalization of QPB and HEB dispersions from the EDCs. The bandwidths of QPB and HEB are reduced to $\sim$ 100 meV at 90 K. For the MDCs, the MDC peak position is energy-dependent at 10 K but becomes nearly energy-independent at 70 K, indicating the formation of a "waterfall" feature. To describe the electron localization behavior more quantitatively, we extracted the band dispersions based on the minimum gradient images (see Fig. S2 in the supplementary materials for details). We then fitted the effective mass ($m_{\rm eff}$) of the QPB using a parabolic band dispersion. As shown in Figs. 3(d) and 3(e), $m_{\rm eff}$ increases rapidly at 60 K and then reaches around 20 times the free electron mass ($m_{\rm free}$) at 100 K. We further show the temperature dependence of the integrated EDCs in Fig. 3(f). It is obvious that the spectral weight transfers from the low-energy (LE) region to the high-energy (HE) region. This spectral weight transfer can be characterized by the ratio of the high-energy spectral weight to the low-energy spectral weight ($I_{\rm HE}/I_{\rm LE}$). The temperature dependence of $I_{\rm HE}/I_{\rm LE}$ is well consistent with that of $m_{\rm eff}$, indicating that the spectral weight transfer and mass renormalization occur synchronously during the electron localization process.

Besides the renormalization of band dispersion and spectral weight transfer, one can observe a significant suppression of density of states near $E_{\rm F}$ in the data shown in Fig. 2, manifesting a pseudogap behavior. We symmetrized the data to better visualize the pseudogap (Fig. 4). It should be noted that this symmetrization operation is not strict due to the presence of a background and the absence of electron–hole symmetry.[34] However, the symmetrization operation remains helpful for identifying the spectral weight suppression at $E_{\rm F}$. As shown in Fig. 4(a), for the H-bulk and H-PSS near 0.9 Å^{-1}, no gap opening was observed at their Fermi crossings. In contrast, for the C-PSS, the opening of a pseudogap could be clearly visualized at the Fermi crossings of the C-PSS. The gap size increases with the development of electron localization [Fig. 4(a)]. Figure 4(b) shows the evolution of symmetrized EDCs during electron localization. While the gap size of the pseudogap gradually increases, the spectral weight of the QPB declines. The pseudogap evolves into a U-shaped insulating gap at 100 K. We performed detailed gap mapping on another $PdCrO_2$ sample. As shown in Figs. 4(c)–4(e), a pseudogap can be observed in all measured cuts across the Fermi pocket. We further extracted EDCs at the Fermi crossings with different polar angles [Fig. 4(f)], which confirms that the pseudogap is isotropic on the circular Fermi pocket of C-PSS.

First, the electron localization phenomenon observed here cannot be explained by simple Anderson localization or photoemission spectrum attenuation caused by disorder or surface degradation. Anderson localization normally causes a suppression of spectral weight near $E_{\rm F}$ while leaving the high-energy spectra unaffected.[35] Surface degradation leads to an overall attenuation of photoemission spectrum intensity, but not a renormalization of the spectral shape. Neither simple Anderson localization nor surface degradation can account for the band dispersion renormalization and spectral weight transfer observed here. Moreover, as shown in Fig. S1 in the supplementary materials, the bulk bands remain sharp after the temperature cycle, which also rules out the presence of random scattering caused by trivial surface degradation. As shown in Figs. 2 and 3, the evolution of photoemission spectra during the electron localization process, including the renormalization of QPB and the spectral weight transfer from QPB to HEB, is strongly related to the mode coupling energy at -0.2 eV. Therefore, to explain the observed electron localization, electron–boson coupling should be considered.

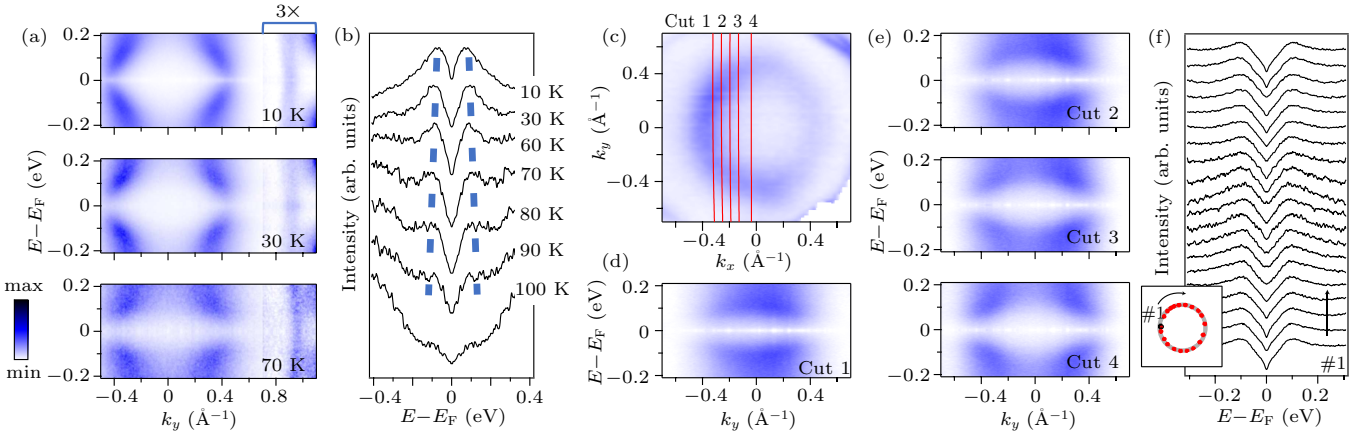


Fig. 4. Pseudogap behavior observed on the Pd surface state in $PdCrO_2$. (a) Symmetrized energy–momentum cuts taken at 10 K, 30 K, 70 K. The photoemission intensity of the right parts of images is enhanced by three times to better show the weak H-PSS and H-bulk states. (b) Temperature dependence of the symmetrized EDCs taken at the Fermi crossings. (c) Fermi surface mapping of the C-PSS. The momentum locations of the energy–momentum cuts are illustrated using red solid lines. (d) Symmetrized energy–momentum cut taken along cut 1. (e) Symmetrized energy–momentum cuts taken along cuts 2, 3, and 4. (f) Symmetrized EDCs taken at the Fermi crossings along the circular Fermi pocket of C-PSS. Inset panel illustrates the momenta of the selected symmetrized EDCs.

We then discuss the origin of this 200 meV energy scale. A previous ARPES study on the surface electronic state of $PdCoO_2$ also observed a kink behavior with an energy scale of approximately 100 meV.[26] It was interpreted as the coupling of electrons with phonons and magnons. Here in $PdCrO_2$ where the energy scale is much higher, from the lattice perspective, phonon energies in the bulk material cannot explain the 200 meV energy scale. Such a high energy may only originate from lattice polarons that evolves multi-phonon excitations. Similar behavior of coupling between surface states and lattice polarons has been observed in various systems.[36,37] In addition to the lattice degree of freedom, magnons could also contribute to the 200 meV energy scale. On the one hand, surface ferromagnetism has been found on the Pd-terminated surface in $PdCoO_2$.[25] Therefore, the magnons may originate from the Pd surface itself. On the other hand, the magnons may originate from the CrO_2 layer that exhibits antiferromagnetism. However, according to previous studies, the coupling between the Pd and CrO_2 layers is relatively weak.[20–22] As observed here and also in previous ARPES studies,[21,22,24–26] no kink behavior was observed on either H-bulk or H-PSS. Unlike the H-bulk and H-PSS that are composed mostly by Pd d electrons, for C-PSS, its orbital configuration is a mixing of Pd, Cr, and O orbitals.[30] Such distinct orbital configuration may lead to an enhancement of its coupling with the magnetic excitations in the CrO_2 layers. Further surface-sensitive experiments that probe phonons or magnons may be needed to verify the origin of the 200 meV energy scale. Nevertheless, our observation of kink behavior on C-PSS clearly indicates that itinerant electrons couple strongly with lattice polarons, magnons, or both in the surface of $PdCrO_2$.

For a system where electrons couple with bosonic modes, different coupling strengths lead to different behaviors of single-particle excitation spectra.[38] In the case of weak coupling, the electron–boson coupling leads to a kink behavior, which is consistent with the phenomenon we observed in the metallic state at 10 K. In the case of strong coupling, the excitation spectra split into two parts: low-energy quasiparticle excitations and high-energy incoherent excitations, resulting in a peak-dip-hump behavior. This is consistent with the photoemission spectra we observed in the near-localized states at 80–100 K. First, we observed a spectral weight transfer from QPB to HEB, which is consistent with the transfer of spectral weight from low-energy quasiparticle excitations to high-energy incoherent excitation. Second, for the HEB at high temperature, its broad peak width and nearly momentum-independent distribution are consistent with the behaviors of incoherent excitations. For the QPB, the MDC peak position at E_F is ~ 0.4 Å^{-1} at 90 K, which is the same as the MDC peak position at E_F at 10 K [Fig. 3(b)], indicating that the MDC peak position at 90 K captures the Fermi crossing of a single-electron-like band. Moreover, the EDC peak width of the QPB at 70 and 90 K increases when the peak moves away from E_F to higher binding energy [Fig. 3(a)], which reflects the change of quasiparticle lifetime with binding energy. It is thereby reasonable to adopt the quasiparticle picture in the description of the QPB at high temperature.

The evolution of photoemission spectra from the kink behavior at 10 K to the peak-dip-hump behavior at 80–100 K suggests that the electron localization on the surface of $PdCrO_2$ is driven by an increase in coupling strength between electrons and lattice/spin excitations. As the coupling strength increases, the electron excitations become coupled to excitations of multiple bosonic modes, leading to the formation of lattice/spin polarons. Such lattice/spin polarons could exhibit an effective mass that is several times larger than the mass of free electrons. Considering that this localization process occurs on the cleaved surface of $PdCrO_2$ irreversibly with increasing temperature or cleavage time (see Fig. S1 in the supplementary materials for details), we consider two possible surface effects: gas adsorption and Pd desorption. It has been found that H or other gas molecules in the vacuum may be adsorbed on the Pd surface.[39] Meanwhile, Pd may also desorb from the surface, forming Pd vacancies.[26] Such adsorption or desorption generates a local potential field near the adsorption sites or vacancies, which could enhance the coupling between electrons and lattice/spin excitations.[40] Besides surface adsorption and desorption, recent scanning tunneling microscopy (STM) studies observed the formation of small Pd clusters on the Pd-terminated surface with a quasi-periodic arrangement.[28,41] Each cluster contains approximately ten Pd atoms. Such cluster formation may lead to a spatial quantum confinement effect, thereby promoting the formation of lattice/spin polarons.

Finally, we discuss the pseudogap behavior. On the one hand, the pseudogap we observed cannot be explained by the surface reconstruction and CDW order that have been found on the Pd-terminated surface.[28,42] First, their reciprocal space wavevectors do not match the size of the circular C-PSS Fermi pocket. Second, the formation of long-range order with a large period would normally lead to a distinct momentum dependence of the energy gap, which is inconsistent with the isotropic gap distribution observed here. On the other hand, a previous ARPES study observed pseudogap behavior on the surface of two-dimensional materials with disordered dopants.[35] The scattering of local impurities or dopants is normally momentum independent, which means that the disorder-induced pseudogap should be equal on all the bands that cross E_F in the Brillouin zone. However, the pseudogap behavior observed here in $PdCrO_2$ is strongly band selective. The pseudogap was observed only on C-PSS but not on H-PSS and H-bulk. We note that the electrons on C-PSS are dragged

by lattice or spin excitations, forming composite polarons with a large effective mass. Therefore, the pseudogap here is better explained as a polaron localization induced by impurities or defects.[43] This scenario explains the band-selective and isotropic momentum dependence of the pseudogap observed here.

In summary, we discovered an electron localization phenomenon on the cleaved surface of $PdCrO_2$. The initial state of the system is a weakly coupled metallic state where electrons couple with spin and lattice degrees of freedom at a characteristic coupling energy of 200 meV. With increasing sample temperature and cleavage time, gas adsorption, Pd desorption, or the formation of small Pd clusters on the Pd surface enhances the coupling strength between electrons and lattice/spin excitations significantly. As a result, the photoemission spectra are renormalized into a high-energy incoherent HEB and a low-energy QPB. The QPB represents the lattice/spin polarons that are composed of dragged electrons and lattice/spin excitations. As the effective mass of polarons increases, the lattice/spin polarons become localized by impurities or defects. The final state system then transitions into a strongly coupled insulating state.

We show that the key characteristics of electronic structure observed in cuprates and other complex oxides, including mass renormalization, the "waterfall" feature, kink, peak-dip-hump, and pseudogap, are universal phenomena that emerge in the electron localization process driven by the coupling among electron, lattice, and spin degrees of freedom. Our data characterize how the low-energy excitation spectra evolve from a weakly coupled delocalized state to a strongly coupled localized state. They provide direct experimental validation for various theoretical models of complex correlated systems focused on the intermediately localized region.

Our results show that the coupling strength between itinerant and correlated electrons can be enhanced by increasing temperature or cleavage time at the surface of $PdCrO_2$. It is then intriguing to further conduct controlled adsorption or desorption experiments to study how adatoms or vacancies play a role in electron localization. It is also worth noting that the average distance between two nearest Pd clusters is around 12 Å.[41] Its corresponding wavevector is around 0.6 $Å^{-1}$, which is close to the momentum positions of the mode-coupling features observed here. Further temperature-dependent STM studies may be required to verify whether there is a correlation between electron localization and the formation of Pd clusters on the surface of $PdCrO_2$.

Acknowledgements

This work was supported by the National Natural Science Foundation of China (Grant No. 12474129) and the National Key Research and Development Program of China (Grant No. 2022YFA1403502). The work at SSRF is supported by the ME2 Project under Contract No.11227901 from the National Natural Science Foundation of China.

References

[1] Imada M, Fujimori A and Tokura Y 1998 *Rev. Mod. Phys.* **70** 1039
[2] Anderson P W 1958 *Phys. Rev.* **109** 1492
[3] Mott N F 1949 *Proc. Phys. Soc. A* **62** 416
[4] Damascelli A, Hussain Z and Shen Z X 2003 *Rev. Mod. Phys.* **75** 473
[5] Anderson P W 1973 *Mater. Res. Bull.* **8** 153
[6] Zaanen J and Gunnarsson O 1989 *Phys. Rev. B* **40** 7391
[7] Schrieffer J R, Wen X G and Zhang S C 1988 *Phys. Rev. Lett.* **60** 944
[8] Mott N F 1990 *Adv. Phys.* **39** 55
[9] Hu C, Zhao J, Gao Q, Yan H, Rong H, Huang J, Liu J, Cai Y, Li C, Chen H, Zhao L, Liu G, Jin C, Xu Z, Xiang T and Zhou X J 2021 *Nat. Commun.* **12** 1356
[10] Xu H C, Zhang Y, Xu M, Peng R, Shen X P, Strocov V N, Shi M, Kobayashi M, Schmitt T, Xie B P and Feng D L 2014 *Phys. Rev. Lett.* **112** 087603
[11] Wang Y, He Y, Wohlfeld K, Hashimoto M, Huang E W, Lu D, Mo S K, Komiya S, Jia C, Moritz B, Shen Z X and Devereaux T P 2020 *Commun. Phys.* **3** 210
[12] Mackenzie A P 2017 *Rep. Prog. Phys.* **80** 032501
[13] Takatsu H and Maeno Y 2010 *J. Cryst. Growth* **312** 3461
[14] Takatsu H, Yoshizawa H, Yonezawa S and Maeno Y 2009 *Phys. Rev. B* **79** 104424
[15] Lechermann F 2018 *Phys. Rev. Mater.* **2** 085004
[16] Lechermann F 2021 *Npj Comput. Mater.* **7** 120
[17] Takatsu H, Nénert G, Kadowaki H, Yoshizawa H, Enderle M, Yonezawa S, Maeno Y, Kim J, Tsuji N, Takata M, Zhao Y, Green M and Broholm C 2014 *Phys. Rev. B* **89** 104408
[18] Le M D, Jeon S, Kolesnikov A I, Voneshen D J, Gibbs A S, Kim J S, Jeong J, Noh H J, Park C, Yu J, Perring T G and Park J G 2018 *Phys. Rev. B* **98** 024429
[19] Sun D, Sokolov D A, Bartlett J M, Sannigrahi J, Khim S, Kushwaha P, Khalyavin D D, Manuel P, Gibbs A S, Takagi H, Mackenzie A P and Hicks C W 2019 *Phys. Rev. B* **100** 094414
[20] Jeon H, Seo H, Seo J, Kim Y H, Choi E S, Jo Y, Lee H N, Ok J M and Kim J S 2024 *Commun. Phys.* **7** 162
[21] Sobota J A, Kim K, Takatsu H, Hashimoto M, Mo S K, Hussain Z, Oguchi T, Shishidou T, Maeno Y, Min B I and Shen Z X 2013 *Phys. Rev. B* **88** 125109
[22] Sunko V, Mazzola F, Kitamura S, Khim S, Kushwaha P, Clark O J, Watson M D, Markovic I, Biswas D, Pourovskii L, Kim T K, Lee T L, Thakur P K, Rosner H, Georges A, Moessner R, Oka T, Mackenzie A P and King P D C 2020 *Sci. Adv.* **6** eaaz0611
[23] Lechermann F and Richter R 2020 *Phys. Rev. Res.* **2** 013352
[24] Noh H J, Jeong J, Jeong J, Cho E J, Kim S B, Kim K, Min B I and Kim H D 2009 *Phys. Rev. Lett.* **102** 256404
[25] Mazzola F, Sunko V, Khim S, Rosner H, Kushwaha P, Clark O J, Bawden L, Markovic I, Kim T K, Hoesch M, Mackenzie A P and King P D C 2018 *Proc. Natl. Acad. Sci. USA* **115** 12956
[26] Mazzola F, Yim C M, Sunko V, Khim S, Kushwaha P, Clark O J, Bawden L, Marković I, Chakraborti D, Kim T K, Hoesch M, Mackenzie A P, Wahl P and King P D C 2022 *npj Quantum Mater.* **7** 20
[27] Sun Z P, Liu Z H, Liu Z T, Liu W L, Zhang F Y, Shen D W, Ye M and Qiao S 2020 *J Synchrotron Rad.* **27** 1388
[28] Wen C, Qin T, Zhang X, Zhang M, Hu W, Shen S, Yang Z, Qi Y, Li G and Yan S 2023 *Phys. Rev. Lett.* **131** 116501
[29] Yim C M, Siemann G R, Stavric S, Khim S, Benedicic I, Murgatroyd P A E, Antonelli T, Watson M D, Mackenzie A P, Picozzi S, King P D C and Wahl P 2024 *Nat. Commun.* **15** 8098
[30] Kim K, Choi H C and Min B I 2009 *Phys. Rev. B* **80** 035116
[31] He Y, Wang Y and Shen Z X 2017 *Rev. Sci. Instrum.* **88** 073903
[32] Graf J, Gweon G H and Lanzara A 2007 *Physica C* **460–462** 194

[33] Bacq-Labreuil B, Fawaz C, Okazaki Y, Obata Y, Cercellier H, Le Fèvre P, Bertran F, Santos-Cottin D, Yamamoto H, Yamada I, Azuma M, Horiba K, Kumigashira H, d'Astuto M, Biermann S and Lenz B 2025 *Phys. Rev. Lett.* **134** 016502

[34] Norman M R, Ding H, Randeria M, Campuzano J C, Yokoya T, Takeuchi T, Takahashi T, Mochiku T, Kadowaki K, Guptasarma P and Hinks D G 1998 *Nature* **392** 157

[35] Ryu S H, Huh M, Park D Y, Jozwiak C, Rotenberg E, Bostwick A and Kim K S 2021 *Nature* **596** 68

[36] Chen C, Avila J, Frantzeskakis E, Levy A and Asensio M C 2015 *Nat. Commun.* **6** 8585

[37] Han T T, Chen L, Cai C, Wang Z G, Wang Y D, Xin Z M and Zhang Y 2021 *Phys. Rev. Lett.* **126** 106602

[38] Gunnarsson O and Rösch O 2008 *J. Phys.: Condens. Matter.* **20** 043201

[39] Li G, Kobayashi H, Taylor J M, Ikeda R, Kubota Y, Kato K, Takata M, Yamamoto T, Toh S, Matsumura S and Kitagawa H 2014 *Nat. Mater.* **13** 802

[40] Reticcioli M, Sokolović I, Schmid M, Diebold U, Setvin M and Franchini C 2019 *Phys. Rev. Lett.* **122** 016805

[41] Yim C M, Zheng Y, Armitage O R, Chakraborti D, Wells C J, Khim S, Mackenzie A P and Wahl P 2025 *Commun. Mater.* **6** 128

[42] Song Q, He Z, Faeth B D, Parzyck C T, Scheid A, Mowers C J, Feng Y, Xu Q, Hasko S, Park J, Barone M R, Suyolcu Y E, van Aken P A, Pamuk B, Fennie C J, King P D C, Shen K M and Schlom D G 2024 *APL Mater.* **12** 081117

[43] Bronold F X and Fehske H 2002 *Phys. Rev. B* **66** 073102